Interaction of Relativistic Electrons with Plasma Facing Components

H.-W. Bartels

IPP 1/269 July 1992

MAX-PLANCK-INSTITUT FÜR PLASMAPHYSIK

8046 GARCHING BEI MÜNCHEN

MAX-PLANCK-INSTITUT FÜR PLASMAPHYSIK

GARCHING BEI MÜNCHEN

Interaction of Relativistic Electrons with Plasma Facing Components

H.-W. Bartels

IPP 1/269 July 1992

Die nachstehende Arbeit wurde im Rahmen des Vertrages zwischen dem Max-Planck-Institut für Plasmaphysik und der Europäischen Atomgemeinschaft über die Zusammenarbeit auf dem Gebiete der Plasmaphysik durchgeführt.

Interaction of Relativistic Electrons with Plasma Facing Components

H.-W. Bartels, IPP Garching
July, 10, 1992

Abstract

Runaway electrons can cause severe damage to plasma facing components of large tokamaks. The designs proposed for the first wall and divertor of the next large fusion experiment, ITER (International Thermonuclear Experimental Reactor), are investigated. Energies of up to 300 MeV per electron and surface energy depositions of 30 MJ/m^2 are assumed. The GEANT code originating from high energy physics was used to model the energy deposition $[J/cm^3]$ quantitatively as a function of the penetration depth and material. A two dimensional representation of the geometry was chosen. For the third coordinate the assumption of symmetric conditions is very close to reality. The magnetic field was included in the analysis. It causes bending back of reflected charged particles and reduced penetration depth of the electrons due to the gyration of the electrons around the magnetic field lines. The energy deposition in the bulk material for a given surface energy load is roughly independent of the incident angle and energy (above 100 MeV) since the main physical process of the energy loss is the formation of an electromagnetic shower, i.e. rapid dissipation of the initial energy into many electrons, positrons and photons. Typical divertor designs protect the cooling tubes with a 1 cm thick graphite layer. Melting of such molybdenum (copper) cooling tubes occurs at a heat load of 50 (25) MJ/m^2. Every additional cm of graphite roughly doubles the runaway protection. Since it is proposed to operate ITER with low cooling water temperatures ($T_{H_2O} < 150°C$), water pressurization due to runaway electron impact is not a serious problem if the cooling pipes do not melt. If the first material facing the plasma is metallic, melting must be expected for heat loads of around 20 MJ/m^2.

1 Introduction

Among many other design restrictions on plasma facing components, runaway electrons are of serious concern since some of the first wall damage to existing tokamaks is caused by generation of a beam of high energy electrons during thermal quench of a disruption. The electrical resistance of electrons in a plasma decreases with energy. Therefore,it is possible to have some electrons in the high energy part of the thermal Gaussian spectrum which gain more energy in an electric field than they lose by friction. The maximal energy of an electron for a given constant loop voltage in the plasma chamber is limited either by the synchrotron radiation (radiated energy per loop less than or equal to the gain from the loop voltage) or by the time available for acceleration (volt-seconds).

For the next step fusion experiment, ITER (International Thermonuclear Experimental Reactor), one expects runaway electrons with energies of up to 300 MeV and surface energy loads of 30 MJ/m^2 during the current quench which lasts roughly 20 ms [1]. Some authors even expect incident energy depositions of up to 100 MJ/m^2 for the first wall [2].

The aim of this report is to predict the energy distribution in plasma facing components caused by the impact of runaway electrons. A short overview of the generation of runaway electrons is given. One section describes the most important physics processes involved in the energy loss of relativistic electrons penetrating material. Since it is not possible to calculate the energy distribution analytically, the GEANT [3] computer code is introduced, which is widely used in high energy physics to simulate quantitatively the interaction of high energy particles with matter. According to the finalized CDA (conceptual design activity) of ITER the first four design options of the first wall and divertor for both the physics and technology phases are investigated. The GEANT code intrinsically works in three dimensions, but symmetric conditions were assumed in the poloidal direction, making it a 2-dimensional model, which is very close to reality. After presentation of the results some special cases are discussed.

2 Generation of Runaway Electrons

Since the cross section of electromagnetic processes decreases with increasing energy, particles in a plasma 'feel' smaller friction forces at higher energies. This is the fundamental reason for the existence of runaway electrons in a plasma with an electric field E. Above a critical velocity v_c, electrons gain more energy in the electric field than they lose, which makes them faster and consequently their friction force decreases further and they gain even more energy and so forth. A quantitative overview of runaway production in toroidal plasmas is given in [4]. An important parameter is the so-called Dreicer field E_D, which is the electric field at which thermal electrons would run away (SI units, except T_e [eV]):

$$E_D = \frac{(2+Z)n_e \cdot e^2 \cdot ln\Lambda}{4\pi\epsilon_0^2\, T_e} \sim \frac{n_e}{T_e} \tag{2.1}$$

Z :	plasma ion charge	–
n_e :	electron density	$[m^{-3}]$
$ln\Lambda$:	Coulomb logarithm	–
T_e :	electron temperature	[eV]

With this expression the critical velocity v_c can be written as

$$v_c = \sqrt{\frac{E_D}{E}} v_{th} \sim \sqrt{\frac{n_e}{E}} \tag{2.2}$$

v_{th} : thermal electron velocity [m/s]

For a given electric field E one always has a certain fraction ($v > v_c$) of electrons of the thermal Maxwell distribution which will be transformed to runaway electrons. The only limit is the relativistic argument that v_c has to be smaller than the speed of light. This leads to the following condition for complete runaway electron suppression [5]:

$$\frac{E}{E_D} < \frac{k\, T_e}{m_e\, c^2}. \tag{2.3}$$

Runaway electrons can be formed in tokamaks during start-up, stationary discharges and disruptions. This report concentrates on runaway generation during the current decay of a disruption. The loop voltage during the current decay is generated according to Lenz's rule and is of the order of

$$U_{Loop} = L\frac{dI}{dt}$$

with (see, for example [6])

$$L \approx 1.4\ \mu_0\ R \tag{2.4}$$

L :	inductance	[H]
R :	major radius	[m]

In JET (R = 3 m, L $\approx 5\mu H$) one observes typical current decay times of 20 ms and thus one gets loop voltages of about 1000 V, assuming an average plasma current of $I = I_{max}/2 \approx 3\ MA$ during the current decay. An example of a measured loop voltage during a JET disruption is shown in fig. 2.1. A clear plateau of about 500 V is measured. As mentioned in [6], the loop voltage 'seen' by the plasma is at least twice as high as the measured one. Similar simple estimations yield loop voltages of up to 5000 V for ITER.

One limitation of the maximal electron energies $E_{e^-,max}$ is given by the acceleration time:

$$E_{e^-,max} = \frac{c}{2\pi\ R}\ \tau\ e\ U_{loop} \tag{2.5}$$

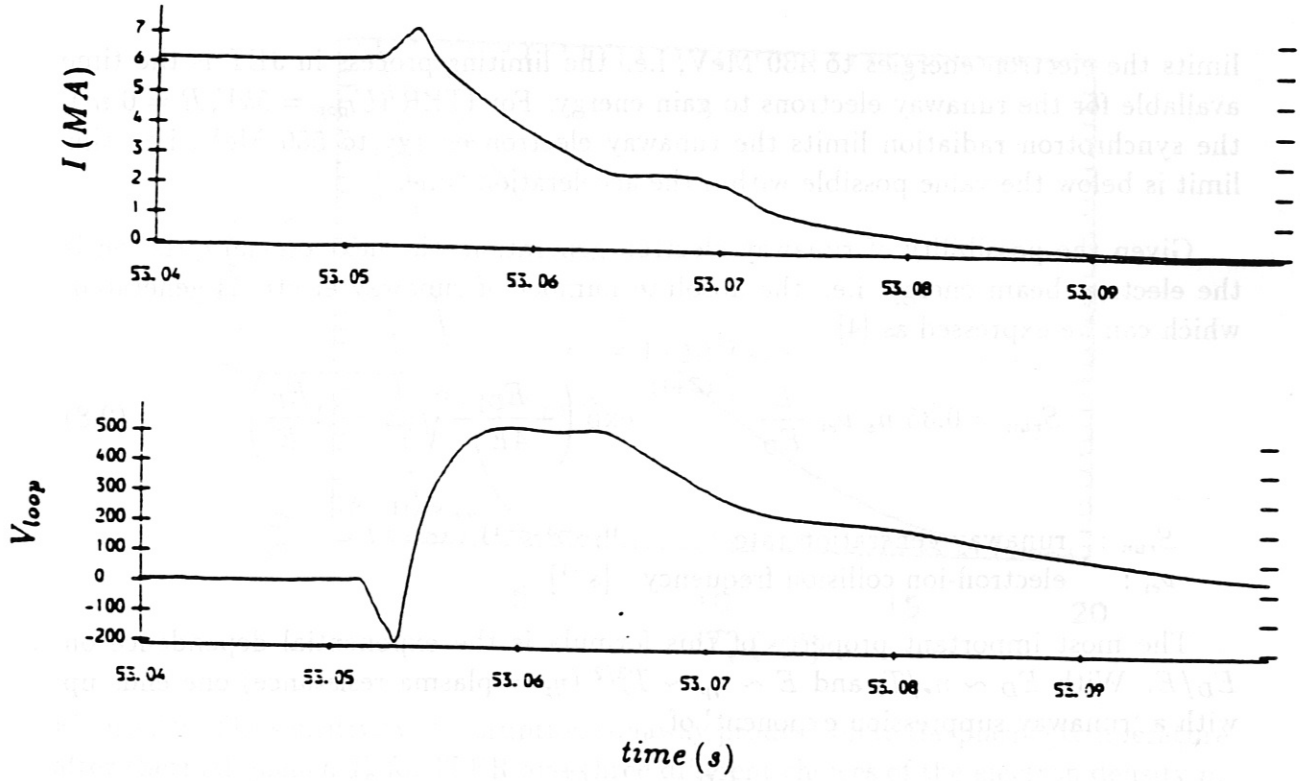

Figure 2.1: Traces of the plasma current and loop voltage for JET shot 18058, a typical carbon limiter disruption.

c :	velocity of electrons $\approx$ speed of light	[m/s]
R :	major radius	[m]
τ :	acceleration time	[s]

With $U_{loop} = L \cdot dI/dt \approx L \cdot I_{max}/2\tau = 1.4\mu_0\ R\ I_{max}/2\tau$ one gets

$$E_{e^-,max} \approx \frac{1.4\ c\ \mu_0\ e}{4\pi}\ I_{max} \tag{2.6}$$

This expression neither depends on the time scale nor on the size of the machine, but exclusively on the size of the plasma current. In JET electron energies of up to 300 MeV can be generated and ITER runaway electrons are limited to 900 MeV by this argument.

Another hard limit is given by the synchrotron radiation emitted by the electrons during their rotation around the torus:

$$\delta E = 90\ E_{e^-}^4/R \tag{2.7}$$

δE :	energy radiated in one gyration	[keV]
E_{e^-} :	electron energy	[GeV]
R :	major radius	[m]

When the electrons radiate as much energy as they gain from the loop voltage, they are obviously not further accelerated. For JET ($U_{loop} = 1\ keV, R = 3\ m$) this

limits the electron energies to 430 MeV, i.e. the limiting process in JET is the time available for the runaway electrons to gain energy. For ITER ($U_{loop} = 5kV, R = 6\ m$), the synchrotron radiation limits the runaway electron energy to 550 MeV, i.e. this limit is below the value possible within the acceleration time.

Given the possibility of runaway electron generation, the next crucial question is the electron beam energy, i.e. the absolute number of runaway electrons generated, which can be expressed as [4]

$$S_{run} = 0.35\ n_e\ \nu_{ei}\ \frac{E}{E_D}^{-\frac{3}{16}(Z+1)}\ \exp\left(-\frac{E_D}{4E} - \sqrt{(Z+1)\frac{E_D}{E}}\right) \tag{2.8}$$

S_{run} :	runaway generation rate	$[m^{-3}\ s^{-1}]$
ν_{ei} :	electron-ion collision frequency	$[s^{-1}]$

The most important property of this formula is the exponential dependence on E_D/E. With $E_D \sim n_e/T_e$ and $E \sim \eta_p \sim T_e^{3/2}$ (η_p = plasma resistance) one ends up with a 'runaway suppression exponent' of

$$\frac{E_D}{E} \sim n_e \sqrt{T_e} \tag{2.9}$$

S_{run} is thus very sensitively dependent on n_e and T_e taken at the end of the thermal quench, where the current decay starts. Varying n_e and T_e in the range of

$$1 < n_e < 3 \quad [10^{-19}\ m^{-3}]$$
$$5 < T_e < 30 \quad [eV]$$

yields generation rates in the range

$$10^{-3} < S_{run} < 10^{20} \quad [m^{-3}s^{-1}]$$

i.e. essentially no runaway production and maximal runaway production (limited by $I_{runaway} < I_{plasma}$). This discussion is not in contradiction to the experimental observations, which vary between runaway production in each disruption (TORE SUPRA), large fluctuation in the runaway production in JET disruptions and the absence of runaways in D-III-D. C Harris [7] performed calculations with a much more detailed description than the simple arguments presented here. Figure 2.2 shows as one result of the calculations the possible total energy content of the electron beams and the single electron energies anticipated for ITER. Given the large uncertainties of the theoretical description, it is necessary to look at experimental data.

Up to now, there have been just indirect measurements of runaway electrons. The first – unpleasant – observation is the damage caused by localized electron beam impact, such as metal melting in JET [8] or cracks in carbon (e.g. TEXTOR [9]).

Another sign of runaway impact is the production of hard X-rays due to bremsstrahlung of the electrons traversing the first wall material (see next section). This phenomenon can be correlated to the end of current decay [10].

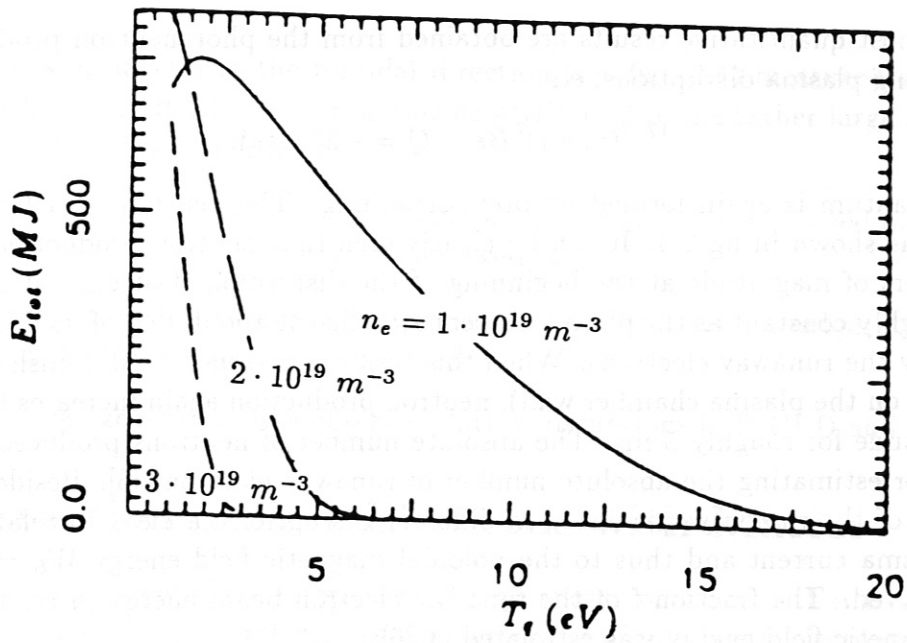

Figure 2.2: The sensitivity of disruption runaway production to the plasma temperature after thermal quench T_q for ITER and three different choices of the electron density n_e [7].

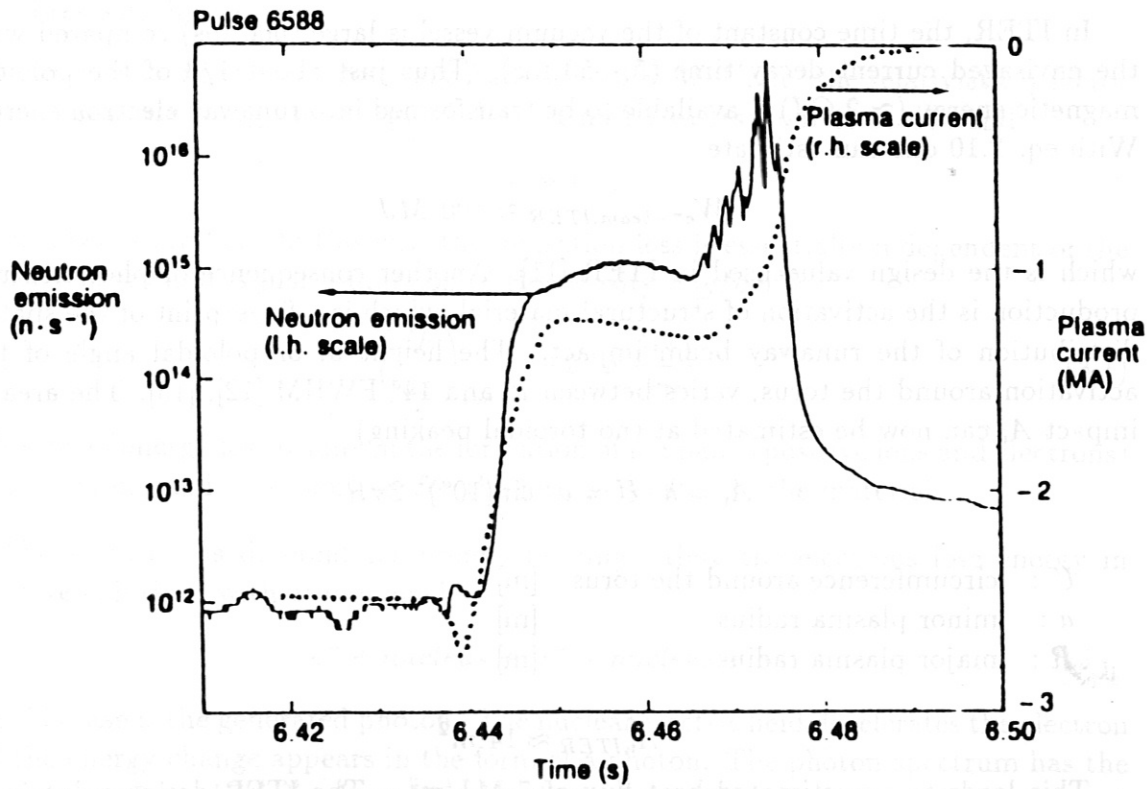

Figure 2.3: Plasma current (dotted) in JET discharge 6588. Also shown is the strength of the neutron production (solid line) on a logarithmic scale. The duration of the neutron pulse coincides with the delay in the plasma current decay. The obvious implication is that a runaway electron current of 1.2 MA has been generated.

The most quantitative results are obtained from the photoneutron production accompanying plasma disruptions, e.g.

$$^{12}C(\gamma, n\alpha)^{7}Be \quad Q = -26\ MeV$$

The γ-quantum is again formed by bremsstrahlung. The neutrons can be measured directly, as shown in fig 2.3. It can be clearly seen that neutron production increases by 2 orders of magnitude at the beginning of the disruption (fast current decay) and stays roughly constant as the plasma current stabilize at about 40% of its original value carried by the runaway electrons. When this residual current also diminish (impact of runaways on the plasma chamber wall), neutron production again increases by 2 orders of magnitude for roughly 5 ms. The absolute number of neutrons produced served as a basis for estimating the absolute number of runaway electrons [6]. Besides a strong variation of the runaways produced in different disruptions, a clear correlation to the total plasma current and thus to the poloidal magnetic field energy $W_B = 1/2\ L\ I^2$ was observed. The fraction f of the runaway electron beam energy in relation to the total magnetic field energy was estimated at [6]:

$$f = 0.03\ I^{0.6} \tag{2.10}$$

I : plasma current [MA]

In ITER, the time constant of the vacuum vessel is large (500 ms) compared with the envisaged current decay time (5 - 50 ms). Thus just about 1/3 of the poloidal magnetic energy ($\approx 2\ GJ$) is available to be transformed into runaway **electron** energy. With eq. 2.10 one can estimate

$$W_{e^{--beam,ITER}} \approx 100\ MJ$$

which is the design value used in ITER [11]. Another consequence of photoneutron production is the activation of structural material, which is a fingerprint of the spatial distribution of the runaway beam impact. The height h, or poloidal angle of the activation around the torus, varies between 7° and 14° FWHM [12], [13]. The area of impact A_i can now be estimated at (no toroidal peaking)

$$A_i = h \cdot U = a \cdot \sin(10^o) \cdot 2\pi R$$

U :	circumference around the torus	[m]
a :	minor plasma radius	[m]
R :	major plasma radius	[m]

$$A_{i,ITER} \approx 14\ m^2$$

This leads to an estimated heat flux of 7 MJ/m^2 . The ITER design value is 30 MJ/m^2 [11], as based on the conservative assumption of a beam height of 10 cm measured in TORE SUPRA [13].

This most important parameter is subject to the following uncertainties:

- The peaking factors in the toroidal direction (see fig. 2.4) measured at TORE SUPRA are about 20, a factor of 4 being attributed to the rather large magnetic field ripple in this experiment.
- The electron beam energy scaling found at JET (eq. 2.10) was based on average beam energies; higher energies are observed too.
- Fewer runaway electrons are observed in the case of divertor configurations [14], [10] and the Be coated first wall of JET.
- No runaway generation was observed during disruptions in D-III-D and ASDEX.

3 Interaction of Fast Electrons with Matter

A comprehensive review of the interaction of high energy particles with matter can be found in [15]. Here the most relevant physics processes of relativistic electrons traversing matter should be summarized. Electrons penetrating matter lose their energy by two processes:

1. ionization loss,
2. bremsstrahlung.

The electron energies of interest vary from 20 to 300 MeV, i.e. the relativistic γ-factor (ratio of particle energy to energy of the rest mass) varies from 40 to 600 and

$$\gamma \gg 1$$

is thus always fulfilled. In this case the ionisation loss is essentially independent of the particle energy and is just a function of the density ρ $[g/cm^3]$:

$$\left(\frac{dE}{dx}\right)_{ion} \simeq -2 \cdot \rho \, \frac{MeV}{cm} \tag{3.1}$$

This kind of energy loss results in the formation of ion pairs (positive ions and electrons) in the medium and is responsible for the heat generated in the material.

The situation is different for bremsstrahlung. Here the electrons lose energy in radiative collisions with atomic nuclei:

$$e^- + nucleus \rightarrow e^- + nucleus + \gamma$$

γ in this case is the generated photon. The nuclear electric field decelerates the electron and the energy change appears in the form of a photon. The photon spectrum has the approximate form dE'/E', where E' is the photon energy. Integrated over the spectrum, the total radiation loss of an electron traversing a medium of thickness dx is

$$\left(\frac{dE}{dx}\right)_{rad} = -\frac{E}{X_0} \tag{3.2}$$

Table 3.1: Radiation length X_0 and E_c in various materials

Material	Z	X_0 in cm	E_c in MeV
carbon	6	22.6	100
water	7.2	36.1	72
iron	26	1.74	24
molybdenum	42	0.98	17.5
tungsten	74	0.35	11

where X_0 is called the radiation length of a material. The radiation length is inversely proportional to the density and the atomic number Z, which indicates the very good absorption property of high Z, high density metals such as tungsten. From eq. 2.2 it follows that the average energy of a beam of electrons of initial energy E_0, after traversing a medium of thickness x, will be

$$\langle E \rangle = E_0 \cdot exp\left(-\frac{x}{X_0}\right) \tag{3.3}$$

Thus, the radiation length X_0 may be simply defined as the thickness of the medium which reduces the mean energy of a beam by a factor e.

Since the rate of ionisation energy loss for fast electrons $(dE/dx)_{ion}$ is approximately constant, while the average radiation loss is $(dE/dx)_{rad} \sim E$, it follows that at high energies radiation loss dominates. The critical energy E_c is defined as that at which the two are equal. It can be roughly given as a function of Z:

$$E_c \simeq \frac{600}{Z}\ MeV \tag{3.4}$$

Values of X_0 and E_c in various materials are given in Table 3.1.

The photons generated via bremsstrahlung lose their energy by three processes:

1. photoelectric absorption,
2. Compton scattering,
3. pair production.

The photoelectric absorption dominates at γ-energies below 0.5 MeV (cross section $\sim 1/E^3$). Here the whole energy is transferred to an atomic electron. In Compton scattering (cross section $\sim 1/E$), which is important in the energy range from 0.5 to 5 MeV, just a fraction of the γ-energy is transferred to an electron:

$$\gamma \rightarrow \gamma' + e^-$$

At energies larger than 5 MeV the process of conversion of a high energy photon to an electron-positron pair (in the field of a nucleus to conserve momentum)

$$\gamma \rightarrow e^+ + e^-$$

is closely related to that of electron bremsstrahlung (cross section independent of energy). The attenuation of a beam of high energy photons of intensity I_0 by pair production in an absorber of thickness x is described by

$$I = I_0 \cdot exp\left(-\frac{7}{9}\frac{x}{X_0}\right) \tag{3.5}$$

where X_0 is the above defined radiation length. Positrons (e^+), the antiparticles of the electron (e^-), lose their energy similarly to the electrons with the exception that the ultimate fate of a positron will be annihilation with an electron, releasing the energy of the rest mass of an e^+e^- system (1 MeV) in the form of two or three photons.

For high energy electrons, a dramatic result of the combined phenomena of bremsstrahlung and pair creation is the occurrence of cascade showers, so-called electromagnetic showers. A parent electron will radiate photons, which convert into pairs, which radiate and produce fresh pairs in turn, the particles increasing exponentially with depth in the medium. This process continues until the energy of the shower particles is comparable to or lower than E_c. From this it follows that for electrons with an initial energy $E_0 \gg E_c$ the maximum energy deposition occurs at a depth increasing logarithmically with the primary energy E_0, and thus the shape of the energy deposition is roughly independent of E_0.

Runaway electrons are expected to hit the plasma facing surface at small incident angles in the range from 1 to 5°. Inside the material they undergo numerous transverse Coulomb scattering processes with the atomic nuclei. The resultant distribution in the net angle roughly follows a Gaussian distribution. The root-mean-square (rms) deflection in a layer x of a medium with the radiation length X_0 is given by

$$\Theta_{space}^{rms} = \frac{20\ MeV/c}{p}\sqrt{\frac{x}{X_0}} \quad (radians) \tag{3.6}$$

A small fraction of large-angle scattering processes is underestimated by this formula. For a 100 MeV electron traversing 1 mm of tungsten the width of deflection angles is 3°. The transverse displacement y from a straight path can be written in the form

$$y_{plane}^{rms} = \frac{1}{\sqrt{6}} \cdot x \cdot \Theta_{space}^{rms} \sim x^{3/2} \tag{3.7}$$

It is mainly this effect of multiple scattering which can lead to substantial reflection of electrons hitting material at small angles. A magnetic field parallel to the surface such as is present in all runaway events in tokamaks counteracts this reflection of electrons, since it bends the particles back into the plasma facing components.

4 The GEANT code

Given the discussion of the preceding section, it is clear that an analytical approach to the heat deposition of fast electrons hitting plasma facing components at small incident angles seems to be impossible, since one has to follow up a lot of secondary particles produced, whose history is determined by probabilistic (quantum-mechanical) laws. The simulation of such events can be achieved in computer codes which follow up the primary particle in small steps, computing for each step the energy loss, multiple scattering and generation of secondary particles according to the distribution functions of the probabilistic laws. When the particle has lost all its energy, the code follows up all secondary particles produced, which can again generate new particles etc. Such a code, called GEANT [3], has been developed at CERN, the large European center of high energy physics, and is widely used in that area. It is a typical application of the 'Monte-Carlo' method, where random generators are used to take decisions at every step according to the distribution functions. For complicated problems this method has by far the best convergence properties, which always goes like $1/\sqrt{n}$, where n is the number of trials (statistical behaviour). In our case this means that the accuracy of the energy distribution of electrons hitting the plasma facing components converge to the correct result with $1/\sqrt{n}$ of electrons simulated with the computer code.

The geometry has to be built up by the user and consists of boxes or tubes nested in each other. Magnetic fields are considered too. Many materials and their properties are provided, but additional ones can be defined.

The user has to set up the starting conditions for the space point and momentum of the primary particle. The code then provides the user with the full information about the track of the particle and secondary particles generated.

The first application of the GEANT code to run away events in tokamaks was performed by a Swedish university team [16]. They started with simple models of monolayers of carbon, molybdenum and steel and found that the GEANT code has problems in describing the correct fraction of reflected energy, when small incident angles (1^o) and low energies ($20\ MeV$) are simulated. The reason for this imperfection is that GEANT performs the multiple scattering and associated displacement just every few mm, which for our special application is not accurate enough.

With a straight path the distance to the surface would be

$$d_{surface} = L \cdot sin(\theta_i)$$

where L is the path length of the electron inside the material and θ_i is the incident angle. The Gaussian displacement from the straight path due to multiple scattering y^{rms}_{plane} is proportional to $L^{3/2}$ (eq. 2.7). Thus one can estimate the path length L_c at which a significant fraction of electrons are scattered back to the vacuum:

$$d_{surface} = y^{rms}_{plane} \quad \Rightarrow$$
$$L_c = 0.015 \cdot \theta_i^2 \cdot p^2 \cdot X_0 \tag{4.1}$$

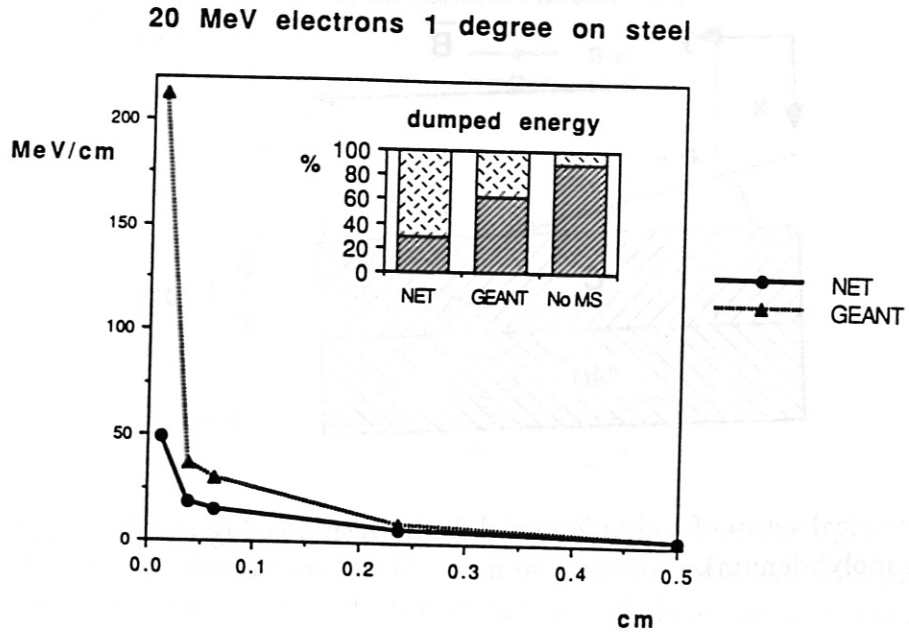

Figure 4.1: Energy deposition of 20 MeV electrons, incident angle 1°, on steel for the uncorrected GEANT code (coarse multiple scattering) and the modified version ('NET', fine multiple scattering).

L_c	critical path length	[cm]
θ_i	incident angle	[rad]
p	momentum of electron	[MeV]
X_0	radiation length	[cm]

For 20 MeV electrons hitting a steel surface at $\theta_i = 1°$ one gets $L_c = 32\ \mu m$, which is much smaller than the distance of a few mm used by GEANT, before the first multiple scattering process is performed. To deal with this imperfection, a small (40 lines) routine was written which simulates the multiple scattering in a proper way. The effect of this routine is shown in fig 4.1, where the energy deposition of 20 MeV electrons (no magnetic field) on steel is shown for unmodified ('GEANT') and modified code ('NET'). In addition, the fractions of dumped and reflected energy are shown for both cases and a simulation excluding multiple scattering effects. The code modification has a large effect on the heat deposition on the surface (factor 4). A different approach to solving the multiple scattering problem in GEANT was performed earlier by [16], yielding results for the test simulation (20 MeV electrons on steel, $\theta_i = 1°$) agreeing 10% with those shown in fig. 4.1 ('NET'-case).

The generation of runaway electrons in tokamaks is inherently coupled with the presence of a strong magnetic field which is roughly parallel to the surface of the plasma facing components. This has two main consequences:

1. Reflected charged particles will be bent back into the material.
2. Charged particles will be forced to gyrate around the magnetic field lines inside the material.

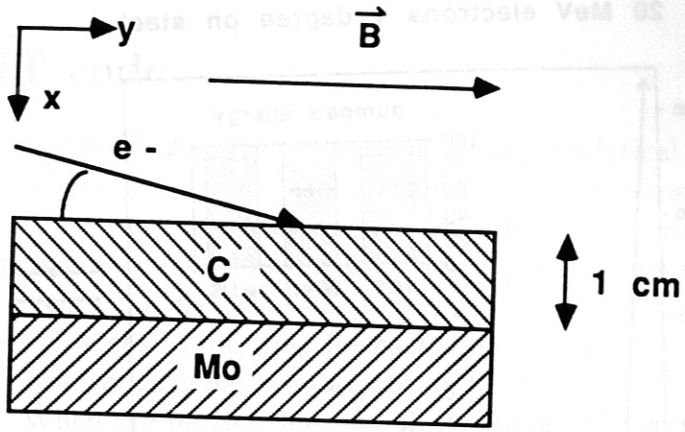

Figure 4.2: Geometrical setup of a simple model for a plasma facing component (1 cm graphite on 1 cm molybdenum).

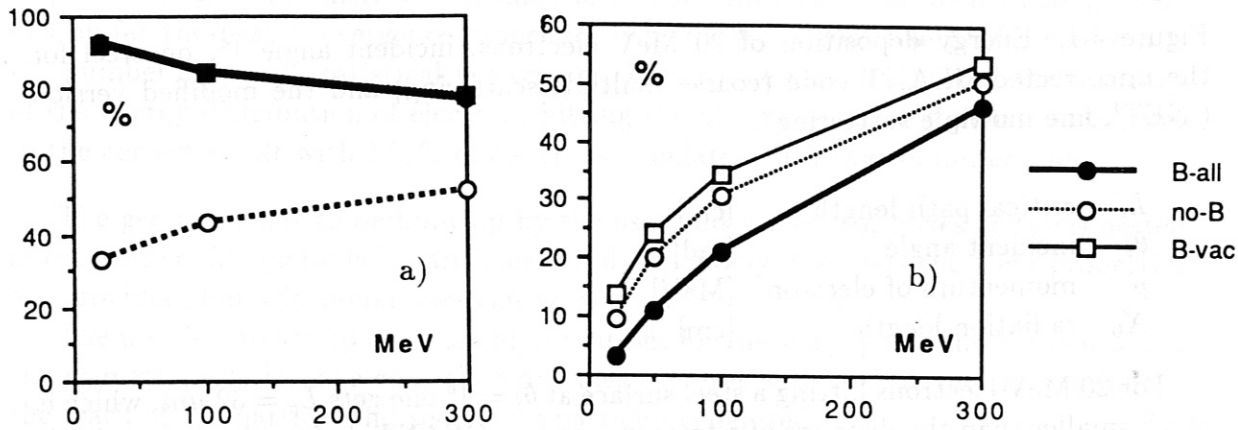

Figure 4.3: The fraction of the runaway electron beam dumped a) into the whole setup (incident angle 1°) and b) into the molybdenum (incident angle 5°) for different assumptions concerning the magnetic field.

The first effect leads to a substantial increase of the energy deposition into the plasma facing components by the runaway beam and the second effect leads to a reduced penetration depth of the electrons. To quantify these findings, simulation of energy deposition of electrons ($\theta_i = 1°$) on a simple two layer model with 1 cm carbon on 1 cm molybdenum (see fig. 4.2) was performed without magnetic field ('no B'), a magnetic field just in the vacuum ('B-vac') to demonstrate the effect of the reflection power, and finally a magnetic field everywhere ('B-all') to show the effect of decreasing penetration depth. In fig. 4.3 the energy deposition in carbon and molybdenum as a function of the incident electron energy is plotted. Neglect of the magnetic field can lead to underestimation of the integral heat deposition by a factor of up to 3 and the peak energy deposition in the metal substrate can be overestimated by a factor of up to 8 when the shielding effect of the magnetic field inside the material is neglected.

It has been argued [17] that the reflected part of the energy, which is bent back

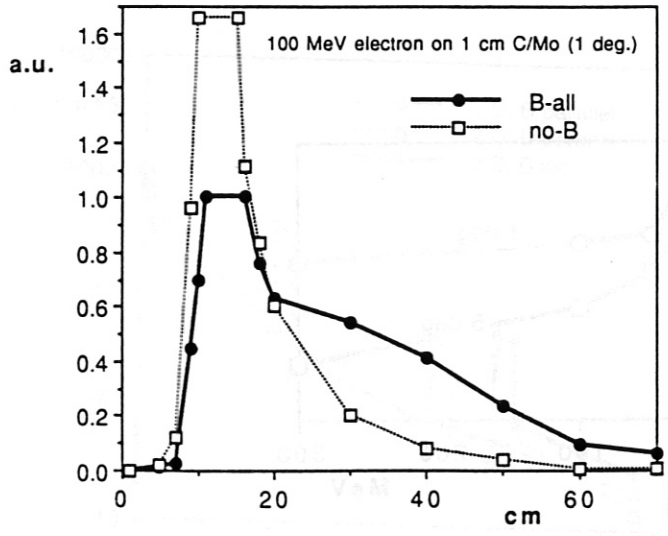

Figure 4.4: Lateral (y-direction, see fig. 4.2) spread of the energy deposition in a molybdenum surface protected by 1 cm of graphite with and without magnetic field. The maximum energy deposition with magnetic field served as normalisation point.

by the magnetic field, will not contribute to the volumetric heating, since the point of second entry into the material may be far away from the beam impact point. To investigate this question the spread of the beam in the y-direction (see fig. 4.2) is shown in fig. 4.4. Starting with a uniform distribution of 100 MeV electrons ($\theta_i = 1^o$) with a width of 2 cm, the width of the beam is shown for the first 250 μm in molybdenum. One can clearly observe the effect of the magnetic field leading to a long tail of the initial peaked distribution. About 60% of the dumped electron energy is spread over 10 cm, and about 90% over 50 cm. It is worth mentioning that the position of the peak of the lateral energy distribution at the molybdenum surface is not at the place where it would be expected for a straight path of the electrons, but rather is shifted due to multiple scattering. The horizontal (z-direction, see fig. 4.2) spread is shown in fig. 4.5. Starting with no beam spread in the z-direction, one ends up with a typical width of 2 cm (root mean square) after penetration of 1 cm of graphite.

In fig. 4.6a the first option design of the divertor plates for the physics phase of ITER is shown. For simplicity, this geometry is sometimes translated into a simple one dimensional layer model and effective thicknesses are introduced, as shown in fig. 4.6b. The effect of this simplification can be a significant underestimation of the peak heat loads in the cooling tubes, since the minimal distance of the cooling tubes from the surface is artificially increased in the one dimensional model. The magnetic field is usually assumed to be parallel to the surface, whereas in reality a small inclination angle is possible, leading to a change in the energy deposition pattern. Figure 4.7 shows both the underestimation of the peak energy deposition of one dimensional models and the effect of an inclined magnetic field ($+2^o$, pointing into the material). The peak heat density deposition in the cooling tube (cooling water) is underestimated by 70% (85%) by neglecting two dimensional geometry and a small inclination of the magnetic field. To avoid this, all simulations of runaway electrons hitting ITER plasma facing components are modelled in two dimensions with an inclined magnetic field (2^o).

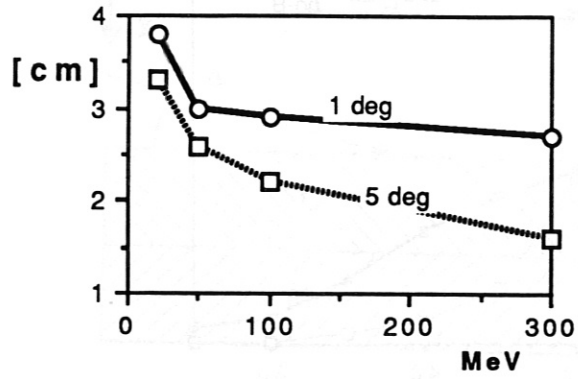

Figure 4.5: Perpendicular (z-direction, see fig. 4.2) spread of the runaway electron beam after penetration of 1 cm of graphite. Twice the root mean square of the spacial distribution is plotted versus the electron energy.

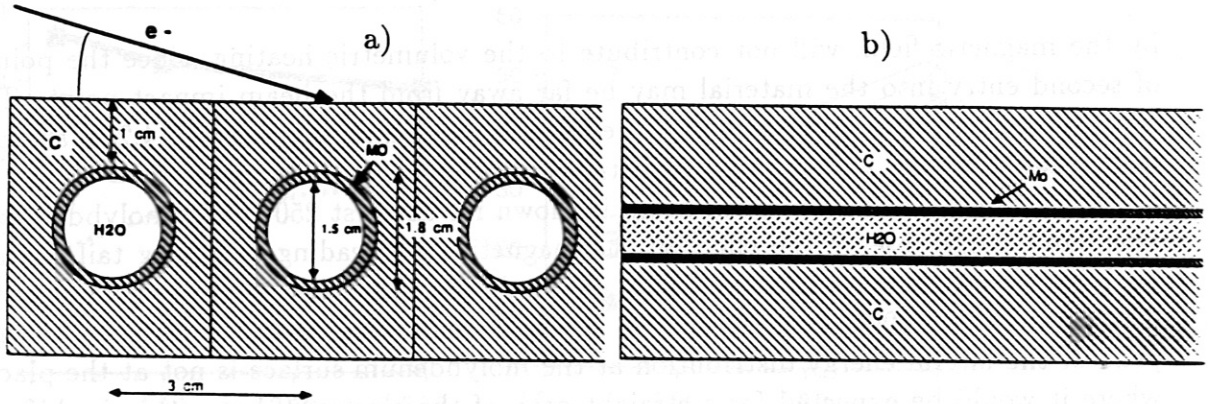

Figure 4.6: The graphite/molybdenum monoblock divertor design for the physics phase of ITER in a) 2 dimensions and in b) a 1 dimensional simplification.

Since the energy deposition of the runaway electron beam is decribed in a statistical manner, the results of the simulation have a statistical and a systematic error. The first is determined by the number of electrons simulated. At IPP-Garching computer center about 30 minutes of IBM-3090 CPU-time is needed for a single simulation to get an accuracy below 10% . The systematic error is determined by the accuracy of the cross sections used for the various physical processes ($\leq 5\%$) and the numerical impacts of the stepping procedure ($\leq 20\%$), which are mainly determined by the choice of the minimal energy loss per step and the lower energy cut for stopping a particle (200 keV for electrons and 10 keV for photons).

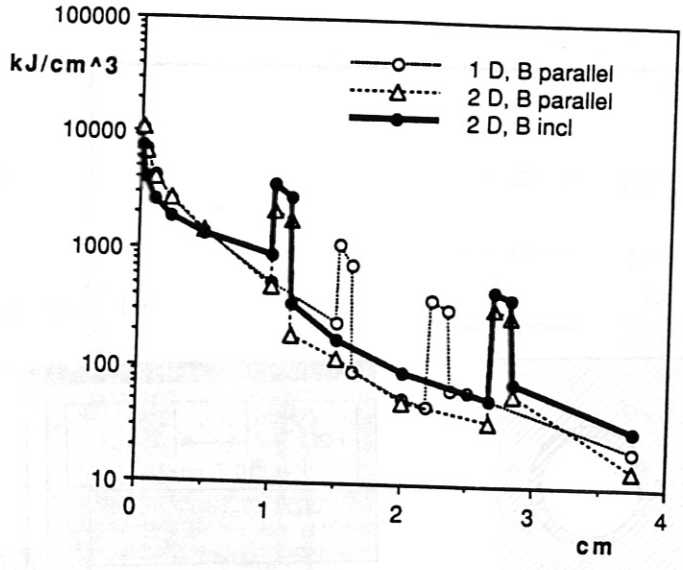

Figure 4.7: The effect of geometrical simplification and inclination of the magnetic field lines (2°) relative to the surface on the energy deposition of a runaway electron beam with heat load 30 MJ/m^2, single electron energy 100 MeV and inclination angle 1°. The energy deposition is plotted versus the penetration depth (x-direction, see fig. 4.2) through the middle of a cooling tube.

5 Models and Results

The ITER operational phase will be subdivided into two parts: the physics and technology phases. The main difference between these phases are the burn times envisaged, that for the physics phase (0.03 a) being much shorter than that for the technology phase (up to 3 a). Consequently, different designs are planned for the two phases. Whereas carbon tiles are planned during the physics phase, tungsten coating is a design option for the technology phase [18], since carbon based materials suffer from strong erosion during normal operation and disruptions. Figure 5.1a-d shows the main features of the ITER first wall and divertor for the physics and technology phases.

Simulations of runaway electron impact on these structures are performed for incident angles of 1° to 5° and electron energies in the range from 20 to 600 MeV. The results are always shown as energy deposition per volume (J/cm^3) as a function of penetration depth through the center of the cooling tubes. The basic assumption is always a uniform electron beam with surface energy deposition of 30 MJ/m^2 [11].

As already shown in fig 4.7, the volumetric energy deposition can strongly vary with the penetration depth. Therefore one can get quite different 'peak' values of the energy deposition for different integration lengths. To deal with this, the typical time scale of the impact of runaway electrons was taken to be 5 ms (see, for example, [11], [6]). On the assumption of a narrow heat deposition at the surface at time $t = 0$, this heat pulse will propagate by thermal diffusion and form a Gaussian distribution with a width σ_t of

$$\sigma_t = \sqrt{\frac{2 \cdot t \cdot \kappa}{\rho \cdot c}}$$

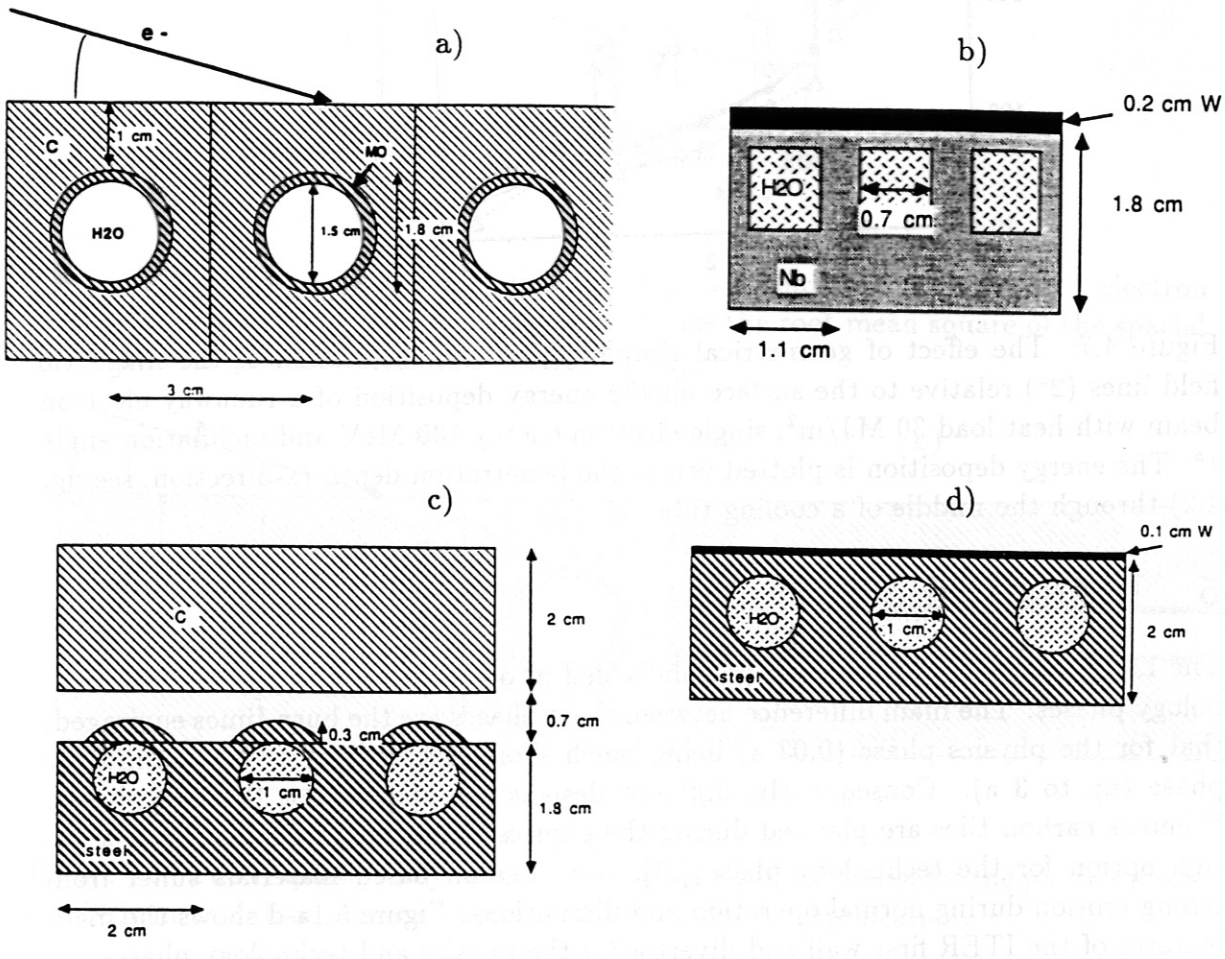

Fig. 5.1: The designs proposed for the ITER plasma facing components during the conceptual design activities (CDA): a) monoblock divertor for the physics phase, b) W-Nb divertor for the technology phase, c) first wall with radiatively cooled tiles for the physics phase and d) first wall covered by a thin W coating for the technology phase.

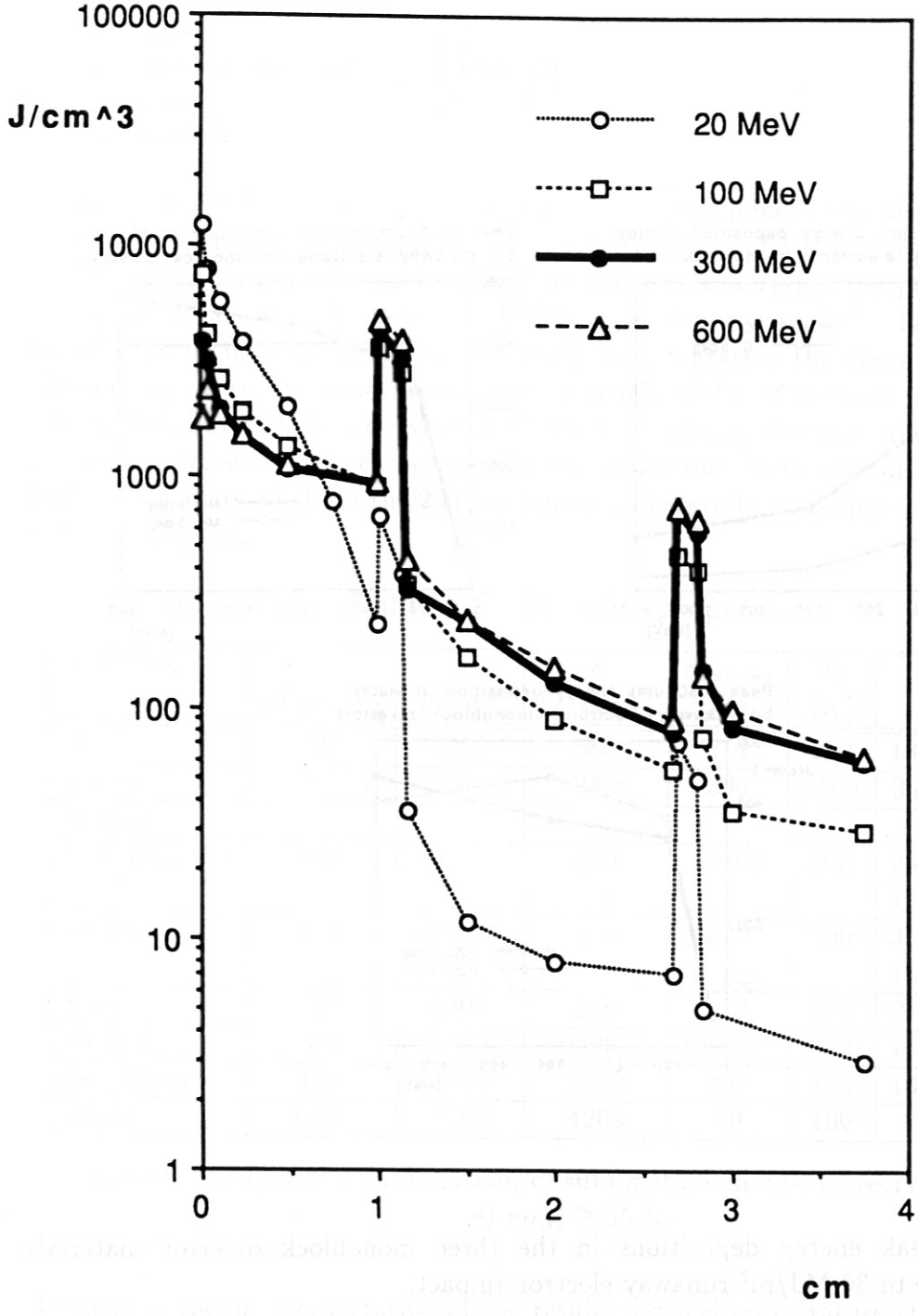

Figure 5.2: Energy deposition versus penetration depth for the monoblock divertor when going through the middle of a cooling tube for a runaway electron surface heat load of 30 MJ/m^2 , incident angle of 1° and different single electron energies.

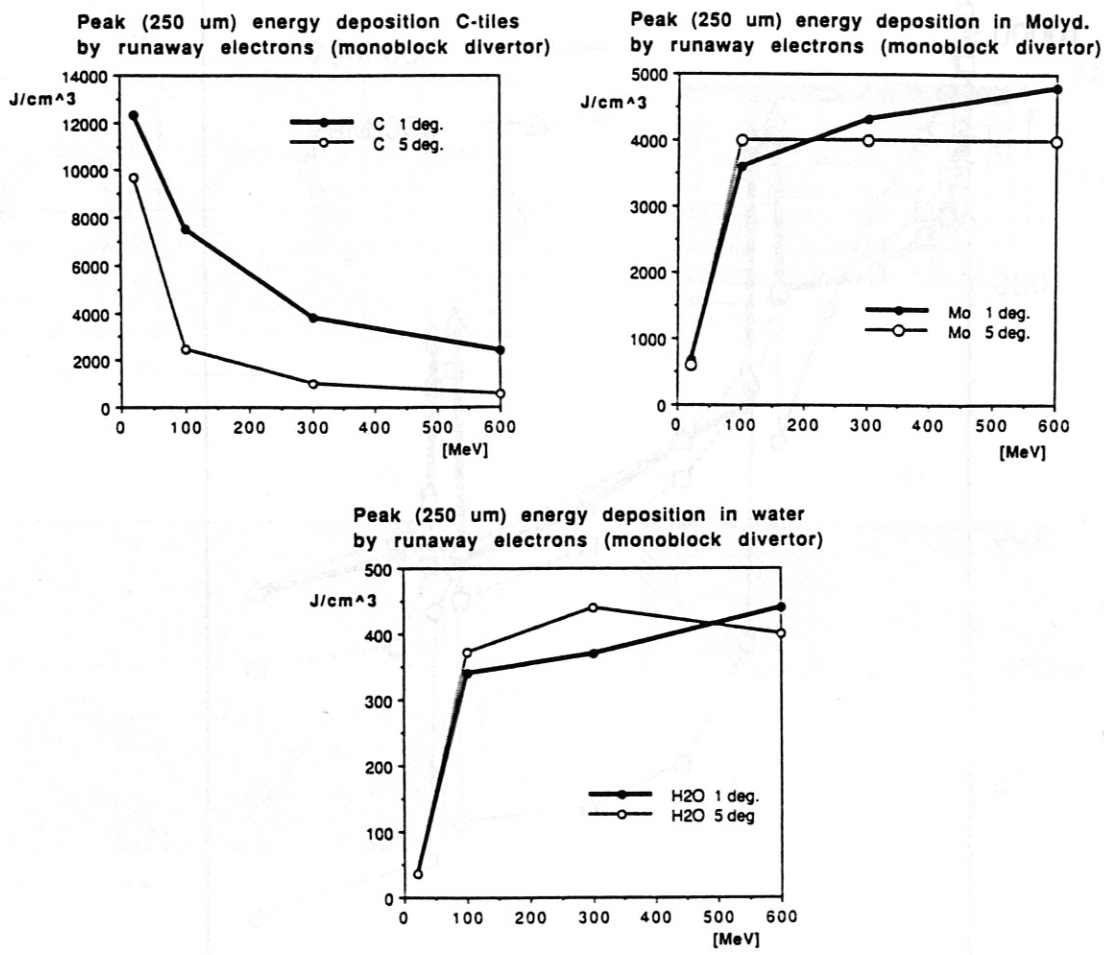

Figure 5.3: Peak energy depositions in the three monoblock divertor materials C/Mo/H_2O due to 30 MJ/m^2 runaway electron impact.

t	time	$[s]$
κ	thermal conductivity	$[W/m\ K]$
ρ	density	$[kg/m^3]$
c	heat capacity	$[J/kg\ K]$

In table 5.1 the Gaussian width $\sigma_{t=5\ ms}$ (typical penetration depths by thermal diffusion are listed for the materials considered. Most of the material properties are taken from [17]. For all structural metals under consideration the penetration depth of a heat pulse varies between 200 and 600 μm (exception Cu). Therefore 250 μm was chosen as interval thickness (bin size), for integrating the deposited energy. For the cooling water, the penetration depth is much smaller if one just considers thermal conduction, but turbulent convection effects will certainly dominate the heat transport, so the bin size was again chosen as 250 μm. Since the bin to bin variations inside the bulk material are small for the 250 μm bin size, the results would not change for smaller bin sizes anyway.

Table 5.1 Material properties

material	κ $[W/m\ K]$	ρ $[kg/m^3]$	c $[J/kg\ K]$	$\sigma_{t=5\ ms}$ $[\mu m]$	T_1 $[K]$	T_2 $[K]$	ϵ_c $[J/cm^3]$
steel	20	7960	550	214	250	1370[a]	4900
carbon	60	2000	2000	390	1000	3500[b]	10000
carbon							43000[c]
molybdenum	100	10200	300	570	400	2600[a]	6700
						1300[d]	3400
tungsten	110	19300	150	620	900	3400[a]	7200
						1500[d]	1700
niob	55	8500	350	430	650	2400[a]	5200
copper	380	8300	400	1100	300	1100[a]	2700
beryllium	100	1850	2600	450	700	1300[a]	2900
water	0.64	1000	4200	40	100	140[e]	600

a) melting, b) strong sublimation, c) sublimation energy, d) recrystallization, e) $p_{H_2O} \geq 35\ bar$

To allow a rough interpretation of the results, critical temperature changes are listed in table 5.1 together with the energy densities needed under adiabatic conditions to reach these temperatures. The adiabatic condition is nearly fulfilled in regions which correspond to $\sigma_{t=5\ ms}$, since this is the range of thermal conduction during the runaway impact.

Figure 5.2 shows the energy deposition into the physics phase divertor for 20, 100, 300 and 600 MeV electrons (30 MJ/cm^3) hitting the surface at an incident angle of 1^o. The steps in the distribution of the energy density correspond to the density changes when going from one material to the other, which reflects the proportionablity of the

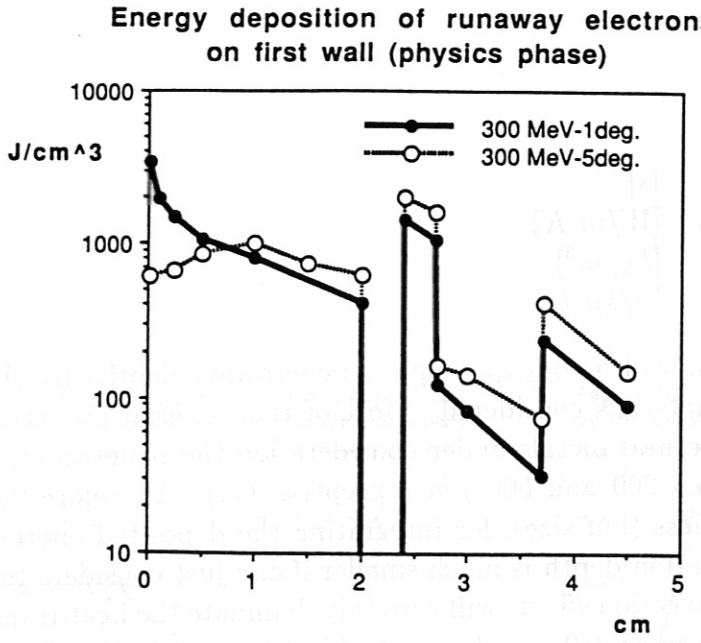

Figure 5.4: Energy deposition of a 30 MJ/m^2, 300 MeV runaway electron beam into the physics phase first wall.

ionisation loss to the density. Since the ratio of the densities of molybdenum and water is roughly the same as that of the critical energy densities ϵ_c of molybdenum and water, a design capable of withstanding tube melting will also avoid problems with cooling water pressurisation. The energy deposition profile is very similar for electron energies above 100 MeV, which is the energy above which the formation of an electromagnetic shower dominates the energy loss. The critical energy densities are reached at about 50 MJ/m^2.

Figure 5.3 shows the peak energy densities in carbon, molybdenum and water for different electron energies and angles. Apart from on the surface (carbon) and low energies (20 MeV), the energy densities deposited in the cooling tube and water are rather independent of the incident electron energy and angle.

For the first wall of the physics phase of ITER fig. 5.4 shows the energy deposition of 300 MeV electrons. The energy densities in the cooling tubes are significantly smaller than in the divertor case, which is due to the thicker carbon tiles (2 cm instead of 1 cm). Melting of metallic structures would start at about 100 MJ/m^2.

Figure 5.5 shows results of an extremely different design solution for the plasma facing components, based on high Z material, i.e. tungsten coating. In this case one has roughly no dependence on incoming electron energies above 20 MeV, which is due to the fact that electromagnetic shower development is already the dominant process above an electron energy of 10 MeV. The high 'stopping power' of tungsten would lead to melting of the structure above 15 MW/m^2. On the other hand, the structure behind the tungsten coating is very well protected. The same trend can be observed in fig. 5.6, where the energy deposition of a thin (1 mm) coated first wall is shown. Finally, fig. 5.7 gives a summary of the main PFC's considered in the ITER CDA.

Similar calculations were done earlier by Calén et al. [16] using the Geant code, either without magnetic field or with a magnetic field just in the vacuum. The effect of this omission was discussed in section 4. A temperature increase of $5°C$ in copper

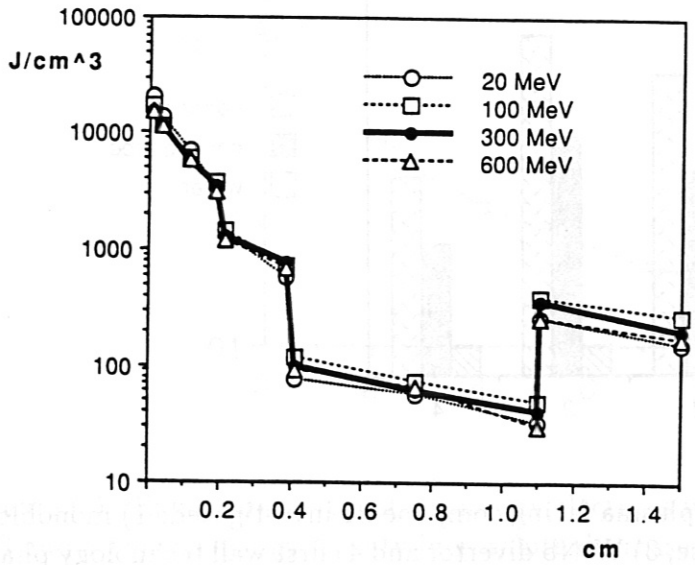

Figure 5.5: Energy deposition of a 30 MJm^2 runaway electron beam (incident angle 1°) into the W-Nb divertor of the technology phase.

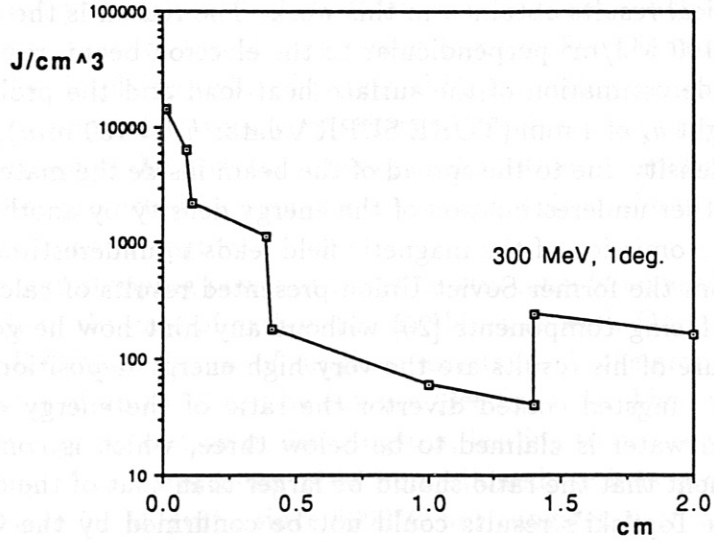

Figure 5.6: Energy deposition of a 30 MJ/m^2 runaway electron beam (incident angle 1°, electron energy 300 MeV) into a tungsten coated first wall of the technology phase.

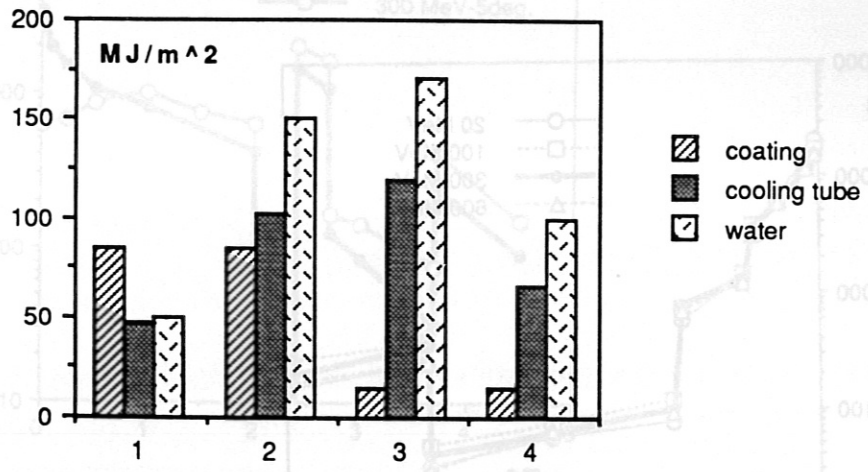

Figure 5.7: Synopsis of all ITER plasma facing components investigated: 1) monoblock divertor, 2) first wall physics phase, 3) W-Nb divertor and 4) first wall technology phase. Shown are the heat loads needed by a runaway electron beam with a single electron energy of 300 MeV, incident angle 1°, to cause severe damage to the coating material (C: strong erosion; W: melting), the cooling tubes (steel, Mo: melting) and the cooling water (H_2O: steam pressurisation).

protected by 1 cm of graphite was reported by a US group [19], [18] for a 100 MJ/m^2 electron beam of 50 MeV electrons (incident angle 5°). This is more than two orders of magnitude away from typical results obtained in this work. The reason is the assumption of a beam energy of 100 MJ/m^2 perpendicular to the electron beam, resulting in a $1/\sin(5^o) \approx 11$ time underestimation of the surface heat load and the problematic assumption of a beam height h_e of 4 mm (TORE SUPRA data: $h_e \approx 100\ mm$), leading to dilution of the energy density due to the spread of the beam inside the material (see fig. 4.5) and thus to a further underestimation of the energy density by another order of magnitudte. Finally, the omission of the magnetic field leads to underestimation by a factor 2. L. Topilski from the former Soviet Union presented results of calculations for typical ITER plasma facing components [20] without any hint how he got those results. The striking feature of his results are the very high energy depositions inside the cooling water. For a tungsten coated divertor the ratio of the energy densities deposited in tungsten and water is claimed to be below three, which is contrary to the simple physical argument that the ratio should be larger than that of the densities ($\rho_W/\rho_{H_2O} = 19.3$). Thus Topilski's results could not be confirmed by the GEANT calculations presented in this report.

6 Special Cases

As already stated in the last section, structural material can be very effectively protected by thick carbon tiles. To quantify the thickness effect, a simple case was considered: 10 cm thick graphite hit by 300 MeV electron at an incident angle of 1°, as

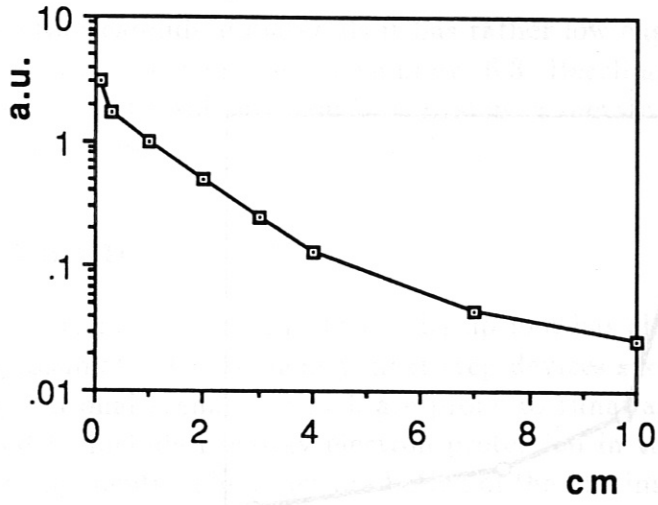

Figure 6.1: Energy deposition by runaway electrons in a thick graphite block. Between 0.3 and 4 cm the energy density in graphite decreases roughly exponentially, i.e. every cm of graphite thickness doubles the runaway protection of structures behind it.

shown in fig 6.1. Between 0.3 and 4.0 cm the distribution is roughly exponential with a decrease of the energy deposition by a factor of 2 for every cm. Since a steel structure at any depth would yield a roughly 4 times higher energy density ($\rho_{steel}/\rho_{carbon} \approx 4$), it can be generally stated that 1 cm of carbon increases the runaway protection by a factor of 2. This is in agreement with the last section when the physics phase divertor (1 cm) and first wall (2 cm) are compared. Another conclusion can be drawn: the end of life conditions of the plasma facing components might show substantial erosion of the C tiles, implying reduced potential in protecting against runaway electrons.

Since copper has very good thermal conductivity, it is a candidate material for cooling tubes in the divertor. Owing to the rather low melting temperatures of copper, such tubes protected by 1 cm carbon would melt at about 25 MJ/m^2 heat load of 300 MeV electrons (1 degree).

The high stopping power of tungsten was considered useful for protecting structures behind it in the case of carbon tile machines as well. One possibility presented during the ITER CDA is the use of tungsten inserts inside the graphite. Additional protection by a factor of up to 20 can be achived (see fig. 6.2). The price for this is high peaking of the energy deposition in the tungsten, leading to melting at about 25 MJ/m^2. Even if melting of the protection rods were allowed, serious problems would arise at heat loads above 50 MJ/m^2 , since 6000°C hot tungsten with a vapour pressure of 10 bar would be formed. Sillage of this liquid tungsten would poison the graphite machine. This would cause degradation of the runaway electron protection due to the use of tungsten rods.

Beryllium is used in JET as a plasma facing material and has shown improved plasma conditions, e.g. due to gettering of oxygen impurities. Disruptions in this beryllium coated machine have a tendency to slower current decay and significantly reduced runaway protection [14]. Owing to the lower melting point of beryllium

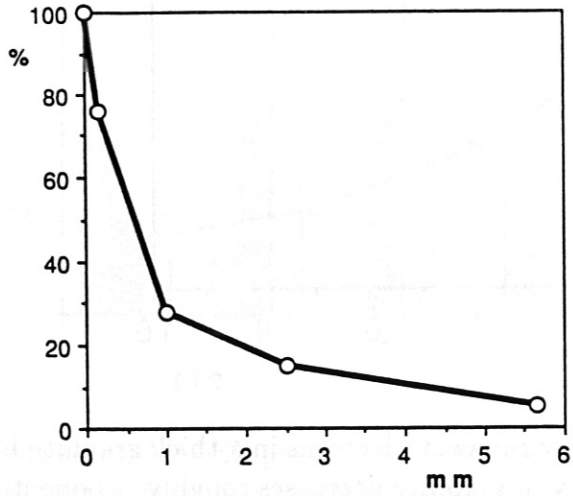

Figure 6.2: Tungsten rods inside the first wall graphite tiles (see fig. 5.1c) lead to substantial reduction of the energy deposition in the first wall steel. Shown is the reduction in % versus the effective tungsten thickness.

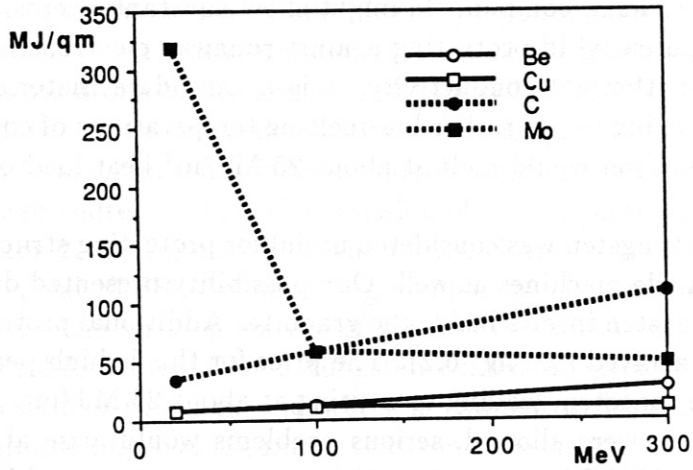

Figure 6.3: Comparison of electron beam heat loads (single electron energy 300 MeV, incident angle 1°) at which severe damage (melting or strong erosion) occurs in a 2 mm Be/Cu and 10 mm C/Mo divertor.

compared with other candidate materials it has rather low engineering protection potential against runaway electrons, as shown in fig. 6.3. Beryllium melting temperatures are already reached at 13 MJ/m^2. Unlike tungsten, a metallic cooling tube behind a (2 mm) beryllium coating is also prone to melting.

7 Conclusion

The production of runaway electrons during disruptions has already caused some damage in existing tokamaks. Consequently, next step devices such as NET or ITER will try to avoid operational scenarios which are prone to runaway production. It is also being attempted to include runaway electron protection in the design criteria of the plasma facing components. The exact prediction of the maximal heat flux envisaged is uncertain owing to the large variation of the runaway generation with electron density and temperature at the end of thermal quench of a disruption. A rough estimation yields a 100 MJ beam energy of up to 300 MeV electrons, leading to about 30 MJ/m^2 heat flux to the plasma facing components if they are properly aligned and the magnetic field ripple is small.

Structural components (e.g. cooling channels) are best protected by thick carbon tiles, e.g. a thickness of 2 (3) cm prevents melting of steel below 100 (200) MJ/m^2 . Copper should be avoided because of its low melting temperature. Inserting tungsten in the carbon tiles to increase the protection of cooling tubes might worsen the runaway electron protection as a result of melting and steam pressurization of the tungsten at rather low heat fluxes (25-50 MJ/m^2). For a bare metallic first wall or divertor, melting has to be envisaged at about 15 MJ/m^2 . On the other hand, a thin tungsten layer (2 mm) affords considerable protection of the structures behind it. The peak energy densities deposited in the cooling water is roughly 10 times as small as in the metal tubes. If the cooling water temperatures are limited to about 100°C (as planned for the next step tokamak), a design capable of withstanding tube melting will also avoid problems with steam pressurization. For reactors working at higher temperatures, the additional heating by runaway electrons may lead to overpressurization of the cooling channels and subsequent loss of coolant accidents. The use of beryllium as first wall coating material would lead to component failure at about 10 MJ/m^2 , but in JET a significant reduction of runaway electron generation has been observed with beryllium coating.

In some machines (ASDEX, DIIID), no disruption generated runaway electrons have been observed, which gives rise to the hope that a proper understanding of the suppression mechanism might solve the problem.

References

[1] International Atomic Energy Agency, 'ITER Conceptual Design Report', ITER Documentation Series No. 18.,Vienna 1991.

[2] G. Vieder, M. Akiba, A. Antipenkov et al., 'Plasma Facing Components for ITER', Thirteenth International Conference on Plasma Physics and Controlled Nuclear Fusion Research, Washington, DC, USA, October 1990.

[3] R. Brun, F. Bruyant, M. Maire, A.C. McPherson, and P. Zanarini, GEANT3, CERN Data Handling Division, 1987.

[4] H. Knoepfel and D.A. Spong, 'Runaway Electrons in Toroidal Discharges', Nuclear Fusion, Vol. 19, No. 6, (1979), p. 785.

[5] J.W. Connor, R.J. Hastie, Nucl. Fusion, Vol. 15, (1979) p. 415.

[6] O.N. Jarvis, G. Sadler and J.L. Thompson, 'Photoneutron Production Accompanying Plasma Disruptions in JET', Nuclear Fusion, Vol 28, No. 11, (1988), p. 1981.

[7] G.R. Harris, 'An Assessment of Major Disruption Characteristics', Final Report of NET Contract 398/89-9 UK, NET Team Garching, Germany, Dec. 1990.

[8] K.J. Dietz, K. Sonneberg, E. Deksnis and R. Shaw, 'Wall Protection in JET', in Tokamak Startup (H. Knoepfel, Ed.), Plenum Press, New York, (1986), 317.

[9] H. Hoven, K. Koizlik et al., 'Material Damage in Graphite by Run-Away Electrons', Journal of Nuclear Materials 162-164, (1989), p.970.

[10] T. Kimura et al., 'Disruption-Induced Hard X-Ray in JT-60', ITER-IL-PH-8-0-23, Garching, 1990.

[11] D.E. Post et al., 'ITER Physics', International Atomic Energy Agency, ITER Documentation Series No. 21, Vienna 1991.

[12] H. Bolt, A. Miyahara, 'Runaway-Electron Materials Interaction Studies', National Institute for Fusion Science, Nagoya 464-01, Japan, (1990).

[13] G. Martin, 'Disruption Induced Run-Away in TORE-SUPRA', ITER-IL-PH-8-0-22, Garching, Germany, 1990.

[14] G.R. Harris, 'Comparisons of the Current Decay During Carbon Bounded and Beryllium Bounded Disruptions in JET', JET Report, JET-R(90)07, Abingdon, Oxon, UK, Dec. 1990.

[15] D.H. Perkins, 'Introduction to High Energy Physics', 3rd edition, Addison-Wesley Publishing Company Inc., (1987), pp. 38-45.

[16] H. Calen et al., 'Further Studies of Energy Deposition from Runaway Electrons in Divertors and First Wall Structures in Tokamaks', Final NET Report 91-263, NET Team, Garching, Germany, 1991.

H. Calen et al., 'Energy Deposition in Tokamaks by Impact of Runaway Electrons', NET-Report, NET Team, Garching, Germany, Nov. 1989.

[17] H. Bolt, E. Zolti et al., 'Effects of Runaway Electron Energy Deposition on Plasma Facing Components', presented at 16th SOFT, London 1990, proc. published in Fusion Technology 1990.

[18] T. Kuroda, G. Vieider et al., 'ITER Plasma Facing Components', International Atomic Energy Agency, ITER Documentation Series, No. 30., Vienna 1991.

[19] US Contribution on Plasma Facing Components, ITER-TN-PC-1-0-U-2, July 1990.

[20] L. Topilski, 'Consequences of Run-Away Electron Influence on the First Wall and Divertor', ITER-IL-PC-6-0-15, July 1990.